Photophysics of dopamine-modified quantum dots and effects on biological systems

SAMUEL J. CLARKE[1], C. ANNETTE HOLLMANN[1], ZHIJUN ZHANG[1], DIANA SUFFERN[2], STEPHEN E. BRADFORTH[2], NADA M. DIMITRIJEVIC[3], WILLIAM G. MINARIK[4] AND JAY L. NADEAU[1]*

[1]Department of Biomedical Engineering, McGill University, Montréal, Québec H3A 2B4, Canada
[2]Department of Chemistry, University of Southern California, Los Angeles, California 90089, USA
[3]Chemistry Division, Argonne National Laboratory, Argonne, Illinois 60439, USA
[4]Department of Earth and Planetary Sciences, McGill University, Montréal, Québec H3A 2B4, Canada
*e-mail: jay.nadeau@mcgill.ca

Published online: 16 April 2006; doi:10.1038/nmat1631

Semiconductor quantum dots (QDs) have been widely used for fluorescent labelling. However, their ability to transfer electrons and holes to biomolecules leads to spectral changes and effects on living systems that have yet to be exploited. Here we report the first cell-based biosensor based on electron transfer between a small molecule (the neurotransmitter dopamine) and CdSe/ZnS QDs. QD–dopamine conjugates label living cells in a redox-sensitive pattern: under reducing conditions, fluorescence is only seen in the cell periphery and lysosomes. As the cell becomes more oxidizing, QD labelling appears in the perinuclear region, including in or on mitochondria. With the most-oxidizing cellular conditions, QD labelling throughout the cell is seen. Phototoxicity results from the creation of singlet oxygen, and can be reduced with antioxidants. This work suggests methods for the creation of phototoxic drugs and for redox-specific fluorescent labelling that are generalizable to any QD conjugated to an electron donor.

Electron transfer between semiconductor nanoparticles and organic molecules bound to their surface is a fundamental process that has been studied extensively for the creation of solar cells and optoelectronic devices (see ref. 1 for a review). When electron transfer occurs, the nanoparticle and its attached molecule exist in highly reactive charged forms long enough to interact with the surrounding environment. The redox potential of the organic molecule can be chosen to maximize the efficiency of charge transfer, or to yield a radical of the desired reactivity able to oxidize a target molecule such as a DNA base[2]. Most work in this area has been carried out with TiO_2 nanocrystallites, and although the possibility of such charge transfer has been established with CdSe and CdSe/ZnS quantum dots (QDs)[3–5], its application to living systems has not yet been reported. The potential for the use of QD–electron-donor systems as biosensors is nonetheless great, as electron transfer eliminates or quenches fluorescence from the particles, thus providing a visible signal of its occurrence[5,6]. In this work, we find that electron transfer between a small molecule (dopamine) and CdSe QDs can be used to create a sensor for physiologically relevant changes in redox potential.

Surprisingly, different sizes (colours) of QDs vary considerably in their ability to bind to and receive electrons from dopamine. To identify the mechanisms behind these observed differences, we carried out all of the experiments with two batches of QDs that demonstrated different photophysics and correspondingly altered bioavailability. Green-emitting QDs (fluorescence emission peak 560 nm) were fully quenched by conjugation to dopamine (>100-fold reduction in emission peak, $n > 5$ conjugations). The presence of the antioxidant β-mercaptoethanol (βME, 5.7 mM) in the conjugate did not affect the quenching. Yellow-emitting QDs (spectral peak 590 nm) were significantly quenched by dopamine conjugation, but to a lesser extent than green QDs (15 ± 2-fold reduction in peak, $n = 5$). There was almost no

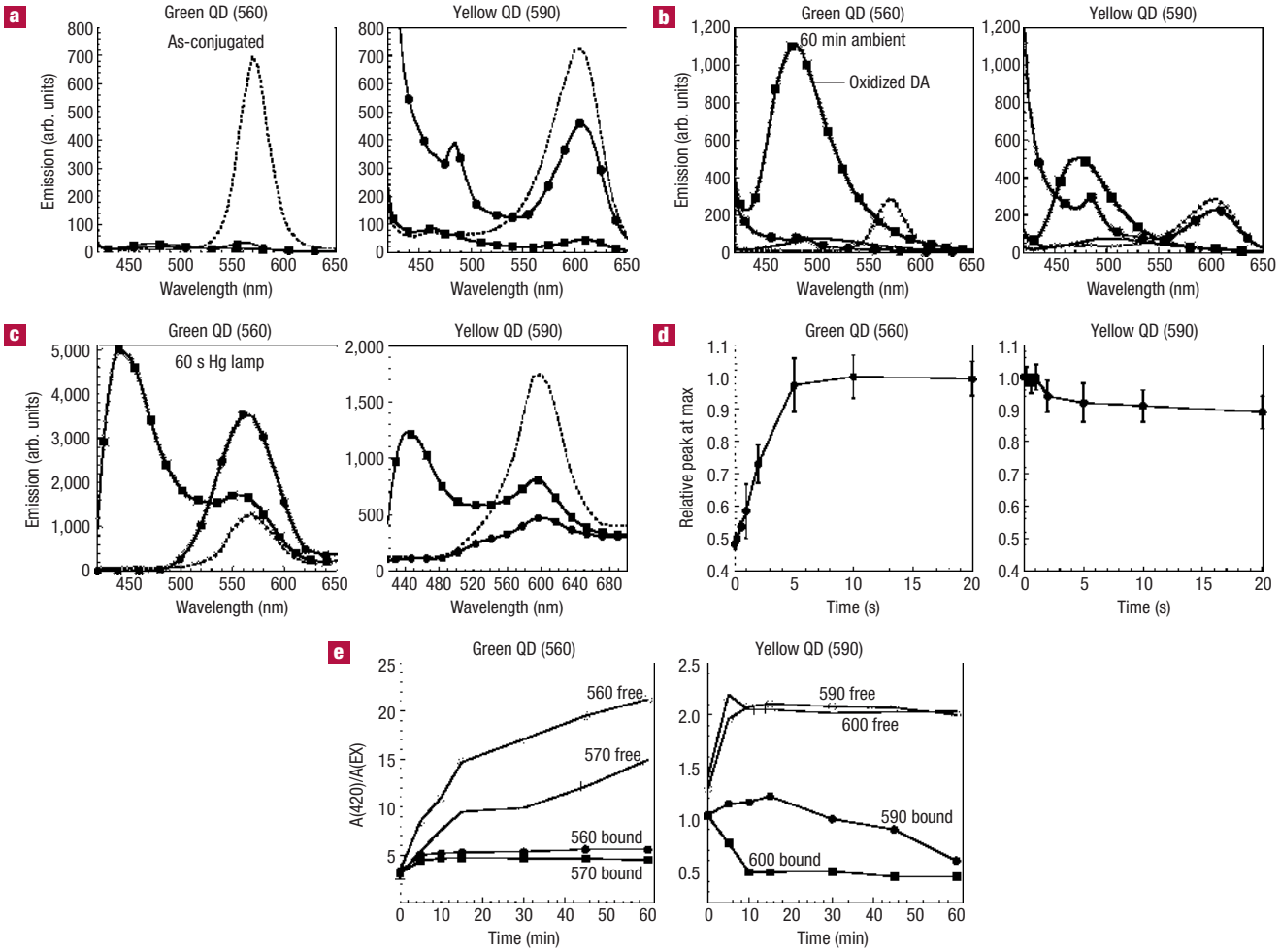

Figure 1 Spectral characteristics of two independent populations of CdSe/ZnS QDs exposed to dopamine. a, Steady-state fluorescence emission intensity in arbitrary units (excitation, 400 nm). MSA-solubilized green QDs (left) and yellow QDs (right) in aqueous solution before conjugation (dotted line), after conjugation to dopamine (filled squares), and after conjugation to dopamine in the presence of βME (filled circles). **b**, After 60 min of exposure to the ambient atmosphere in the dark, a large emission peak at 470 nm, representing oxidized dopamine, is evident in the green QD conjugates without βME (filled squares). This peak is significantly stronger than that of the unconjugated QDs alone (dotted line). The conjugates containing βME (filled circles) remain fully quenched. The spectrum of a 3-mM dopamine solution under the same conditions (straight line) is also shown. An oxidized-dopamine peak also appears in the yellow QD conjugates without βME (filled squares), but it is less than half of the intensity. In yellow QD conjugates containing βME (filled circles), the QD emission intensity is almost equal to that of the QD solution alone (dotted line). **c**, Exposure of a droplet of quenched QD–dopamine to 60 s of high-intensity ultraviolet illumination on a microscope slide, with spectra taken through a liquid-crystal filter. The spectra shown are the sum of the spectra observed with the DAPI and QD filters; thus, the relative heights of the blue and green peaks cannot be quantitatively compared. The original QDs retain their initial spectrum and intensity for at least several minutes under these conditions (dotted line). The green QD conjugate shows intense blue oxidized-dopamine fluorescence in the absence of βME (filled squares), with relatively weak green QD fluorescence. In the presence of βME (filled circles), there is no blue fluorescence and the green QD fluorescence is significantly brighter. Yellow QD–dopamine shows weak yellow fluorescence both with (filled circles) and without (filled squares) βME, with a blue peak in the absence of βME that is weaker than that seen with the green QDs. (Differences in the oxidized-dopamine spectrum with respect to **b** are due to the cut-offs in the microscope filter sets.) **d**, Relative brightness of (10 μm)^2 areas of QD solutions with βME on a slide under Hg lamp illumination. Normalized fluorescence at peak (560 or 590 nm) ± s.e.m. is given for five distinct regions of the illuminated field. The minimal exposure time to obtain a spectrum was 200 ms. **e**, Ratios of absorbance at 420 nm (oxidized dopamine) to QD absorbance at the exciton peak taken for four colours of QDs (green: QD 560 and QD 570; yellow: QD 590 and QD 600) under two independent conditions: 'free' (open symbols), where QD conjugates were prepared with a 2,000: 1 molar ratio of dopamine to QDs, and the solution was not purified; and 'bound' (filled symbols), in which the solution was purified of molecules of MW $<10{,}000$ before each data point. The time points indicate exposure to ultraviolet light (365 nm) for the time indicated. The limit of detection was A(420)/A(EX) ~ 0.5. The data are an average of 2–5 experiments (the standard errors are smaller than the symbols).

quenching of the yellow QDs in the presence of βME (Fig. 1a). The efficiency of dopamine as a quencher was confirmed with collisional quenching experiments, in which dopamine was added to QD solutions without conjugation; quenching of both types of QDs was linear at low concentrations, but at higher concentrations showed downward curvature that could be fitted to the non linear Stern–Volmer equation indicating two subpopulations of emitting sites, only one of which (state a) is accessible to the quencher[7]:

$$\frac{I_0}{\Delta I} = \left(1 + \frac{1}{k_a[\mathrm{DA}]}\right)\frac{1}{f_a},$$

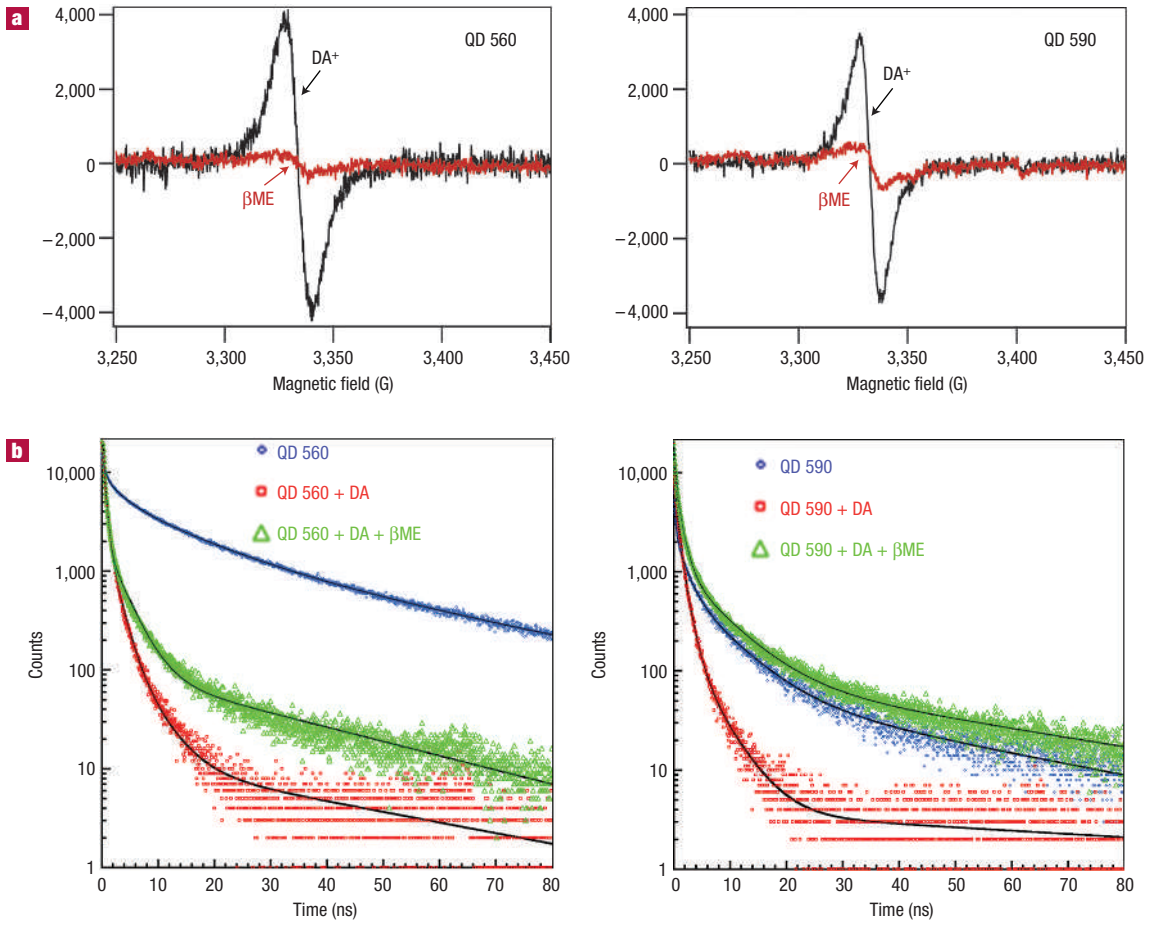

Figure 2 Oxidation of QD–dopamine by EPR and transient emission spectroscopy. a, X-band differential EPR spectra measured at 4.7 K after illumination at 80 K of dopamine-conjugated QDs in the absence (black) and in the presence (red) of βME. Cut-off filter 355 nm; frequency 9.4 GHz. **b**, Time-resolved emission data of unconjugated MSA-solubilized QDs (blue, open circle) and QD–dopamine conjugates in the absence (red, open square) or in the presence of βME (green, open triangle). The solid lines give a 4-exponential fit. Exponential fits showing lifetimes are given in Supplementary Information, Table S1. The data are normalized to peaks at time 0.

where I_0 is the initial fluorescence intensity, $\Delta I = I - I_0$, k_a is the binding constant for state a, [DA] is the dopamine concentration, and f_a is the fraction of sites in state a. The f_a values were comparable for green QDs (0.98 ± 0.02, $n = 3$) and yellow QDs (0.96 ± 0.04, $n = 3$), but the binding constants (0.39 ± 0.03 for green QDs, 0.11 ± 0.02 for yellow QDs) were very different (fits shown in Supplementary Information, Fig. S1).

A strong absorbance peak at 420 nm and a corresponding emission peak at 470 nm, representing the oxidized quinone form of dopamine, appeared slowly in samples after exposure to room air in the dark, and rapidly on light exposure (see Supplementary Information, Fig. S1). This peak appeared more rapidly and strongly in green-emitting than yellow-emitting QD samples; the presence of βME prevented its appearance. This peak was not seen in dopamine solutions without QDs under the same conditions (results after 60 min are shown in Fig. 1b; results after 20 and 120 min are shown in Supplementary Information, Fig. S2).

When a droplet of quenched QDs was placed under microscope ultraviolet–blue illumination without antioxidants, the QD fluorescence remained weak while an oxidized-dopamine peak appeared rapidly. In the presence of βME, however, quenched green QDs showed a striking fluorescence enhancement that occurred over a time course of seconds. The same effect was not seen for yellow QDs, which remained dim under ultraviolet exposure with and without βME (Fig. 1c). This restoration of QD fluorescence was only seen under high-intensity illumination of low concentrations of QDs, not in bulk solutions exposed to a ultraviolet wand, even after 24 h (data not shown; the spectra after 24 h are similar to those in Fig. 1b). The restoration of QD fluorescence was seen as a rapid brightening of the green particles under microscopic examination, reaching a peak in 5–10 s; in contrast, the yellow particles were initially bright, then began to fade during observation (Fig. 1d).

These data suggest that green and yellow QDs interact differently with dopamine, but do not determine whether green QDs are binding more dopamine molecules than yellow QDs, or whether they are just oxidizing them more efficiently. Using ultraviolet–visible spectroscopy, we were able to track the number of oxidized-dopamine molecules per QD in solutions containing both free and bound dopamine as a function of time. This revealed that the number of dopamine molecules bound to green QDs remained constant with time, but that the number bound to yellow QDs decreased to detection limits within 60 min. The loss of conjugated dopamine into the solution correlated with the loss of the ability of the QDs to oxidize free dopamine (Fig. 1e). Two additional colours of QDs, QD 570 and QD 600, were then

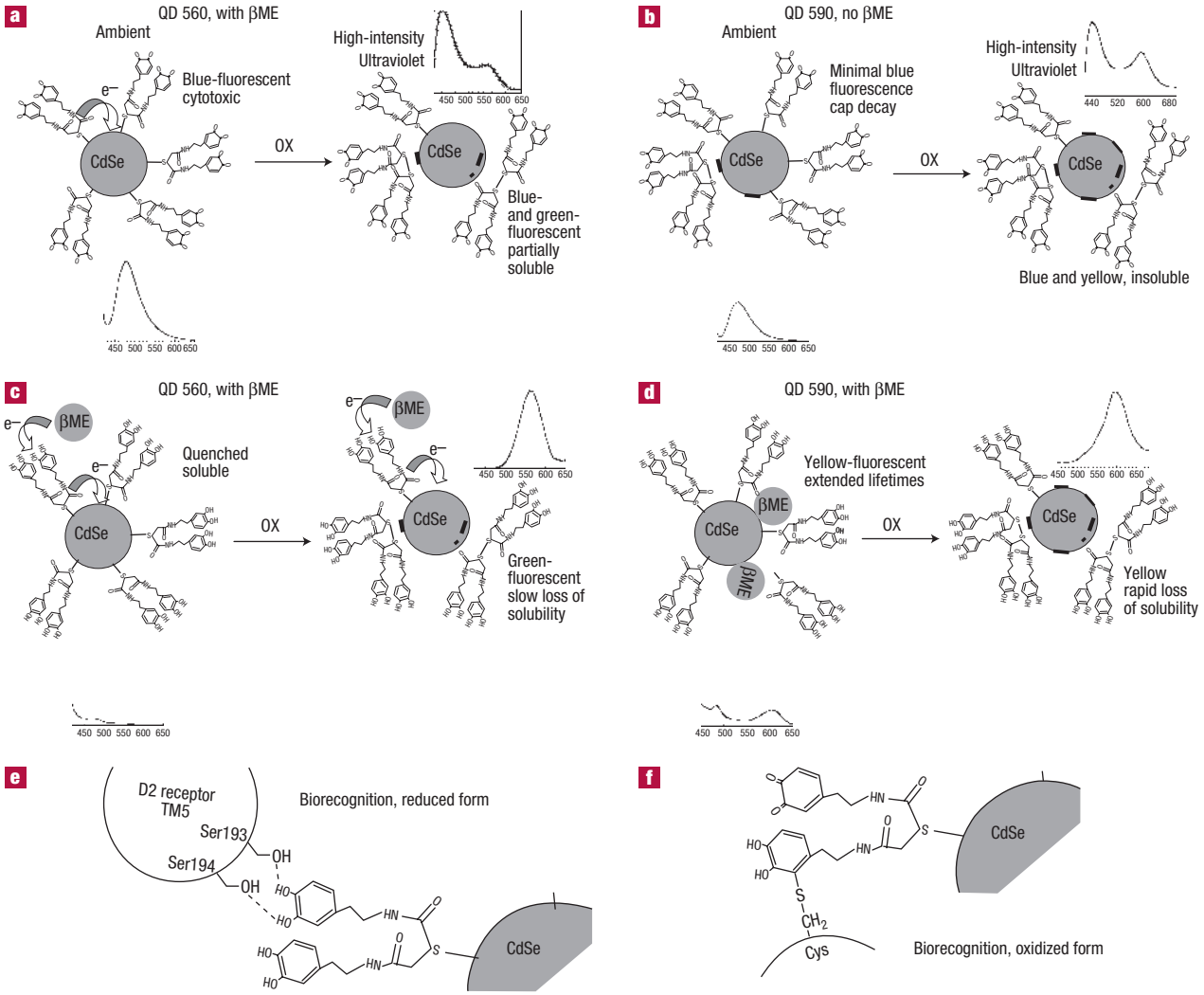

Figure 3 Proposed mechanisms for observed spectral and cell-uptake properties of QD–dopamine conjugates under different environmental conditions. Each of these states can be distinguished by fluorescence spectroscopy; typical spectra are shown in the insets. **a**, Under normal ambient conditions of water and oxygen, but before light exposure ('ambient'), QD 560 oxidizes dopamine, leading to charge separation and quenching of QD fluorescence (corresponding to Fig. 1b). Under oxidizing cellular conditions or high-power ultraviolet exposure ('OX'), cap decay causes loss of the dopamine and corresponding loss of particle solubility, simultaneous with enhanced fluorescence[29] (corresponding to Fig. 1c). The thick black lines indicate the formation of oxides, which passivate the surface and increase fluorescence but reduce solubility. **b**, QD 590 shows essentially the same features, but less generation of oxidized dopamine and more rapid loss of QD solubility. The insoluble, oxidized QDs are incapable of oxidizing dopamine. **c**, In the presence of βME, electron transfer between dopamine and QD 560 is not inhibited, but the generated dopamine radical may be re-reduced. Hence, dopamine remains soluble and attached to the QDs. Photooxidation occurs slowly; so slowly that enhancement of fluorescence is visible under the microscope. **d**, In QD 590, βME interacts directly with QDs and inhibits electron transfer between dopamine and QDs, leading to the appearance of oxidized-dopamine fluorescence and the alteration of QD fluorescence lifetimes. This allows for restoration of QD fluorescence, but loss of solubility and more rapid photooxidation, as well as possible displacement of the dopamine ligand by displacement of the MSA-solubilizing group by the sulphur of the βME. **e**, Specific recognition of reduced QD–dopamine can occur through hydrogen bonding of the catechol hydroxyls to two specific serine residues, Ser 193 and Ser 194, in the fifth transmembrane domain (TM5) of the D2 dopamine receptor. Mechanisms of recognition involving the dopamine amino group are prevented by the conjugation to the QD. **f**, In the case of oxidized QD–dopamine, the highly active quinone can react with cysteines on the dopamine receptor or other proteins. A covalent bond between the sulphhydryl of cysteine and the dopamine is formed.

investigated to confirm the relationship between more energetic excitons and conjugate stability. QD 570 only showed a slight decrease in dopamine-oxidizing power and conjugate stability relative to QD 560; however, QD 600 was remarkably unstable, losing its dopamine cap within 10 min (Fig. 1e). These findings are consistent with recent observations[8] of size-dependent cap decay in CdTe. Future studies will determine the exact mechanisms; our goal for this work was to relate these properties to bioavailability.

Using electron paramagnetic resonance (EPR), we confirmed charge separation in both green and yellow QD conjugates. EPR spectroscopy provides an unambiguous identification of the species involved in the charge-separation processes by revealing changes in local symmetry and hyperfine couplings along the pathway of charge carriers (further information in Supplementary Information, Fig. S3). Illumination ($\lambda > 355$ nm) of dopamine-conjugated QDs leads to the formation of a carbon-centred radical

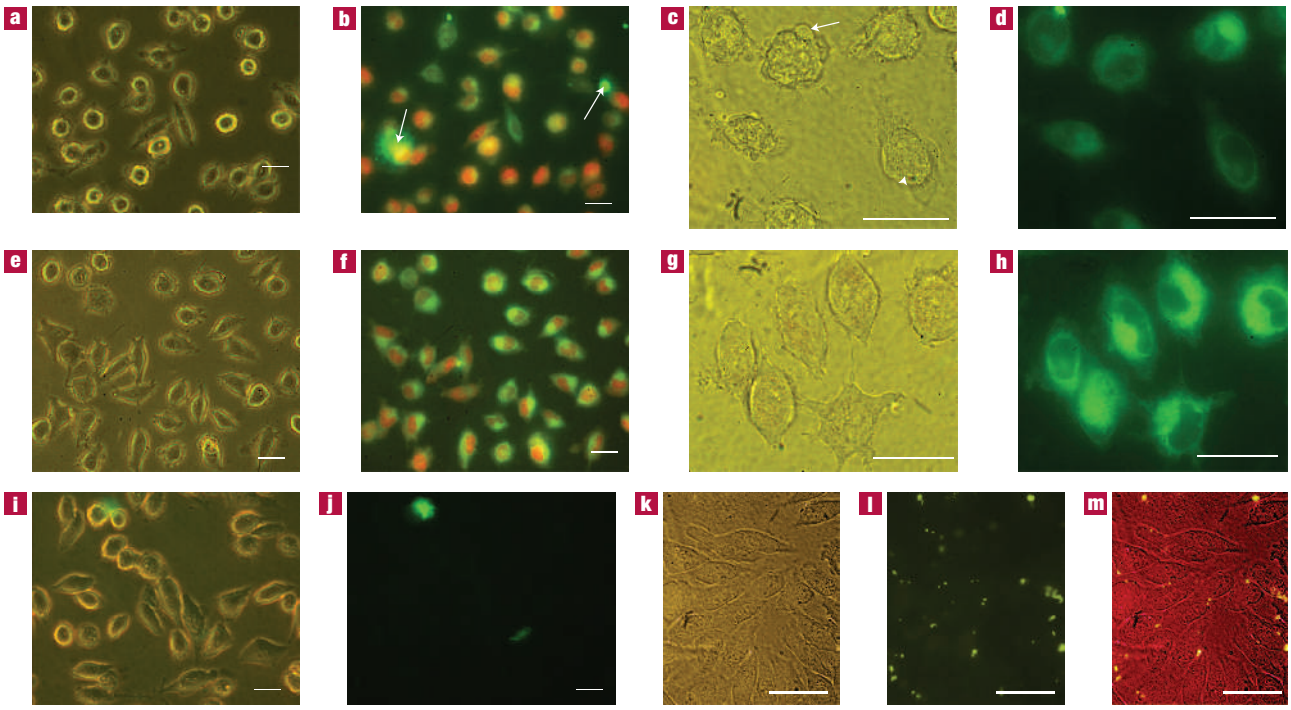

Figure 4 Uptake of QD–dopamine by mammalian cells. Scale bar = 10 μm. Fluorescence images with the same magnification were taken with the same exposure conditions, allowing comparison of the intensities. **a**, Phase-contrasts image of A9 cells stably transfected with human D2 dopamine receptors after incubation with green QD–dopamine in the absence of antioxidants. Note the membrane blebbing (rough edges) and preponderance of round, very bright cells, indicating detachment from the culture dish. **b**, Fluorescence image of cells in **a** co-labelled with the nuclear stain SYTO Red. Note the clusters of unassimilated QDs (arrows) and uneven SYTO Red staining. **c**, High-power brightfield image of cells under the same conditions as **a**. Under this high resolution, signs of cell death are apparent as blebbing (arrow) and nuclear extrusion (arrowhead). **d**, Epifluorescence image of the cells in **c**, showing QD uptake in most of the cell, excluding the nucleus. **e**, Phase-contrast image of A9 cells after incubation with green-QD–dopamine with the addition of 5.7 mM βME. Note the smooth cell edges and the absence of rounded cells. **f**, Epifluorescence of cells in **e** labelled with SYTO Red. Note the even distribution of both the QD and dye labelling and the absence of unassimilated QDs. Also note the perinuclear distribution, with absence of QDs in the cytoplasmic region just inside the cell membrane. **g**, High-power brightfield image of cells under the same conditions as **e**. Cell health is indicated by smooth edges and lamellopodia strongly adhered to the dish. **h**, Fluorescence image of the cells in **g**. Note the brightness of the labelling compared with **d**. **i**, Phase-contrast image/fluorescence overlay of A9 cells incubated with QD–dopamine in the presence of βME and 5-mM unlabelled dopamine. Note the two large clusters of QDs in the background. **j**, Fluorescence-only image of the cells in **i**. **k**, High-power brightfield image of A9 cells after incubation with yellow QD–dopamine with the addition of 5.7-mM βME. The cells seem healthy. **l**, Fluorescence image of cells in **k**, showing QD clusters throughout the medium. **m**, Overlay of **k** and **l**, showing adherence of QD clusters to cell membranes without internalization. The brightfield image was pseudo-coloured to enhance the contrast.

with a g-tensor of 2.003 with a linewidth of $\Delta H_{app} = 16$ G (Fig. 2a). This signal corresponds to the dopamine cation radical (DA^+), exhibiting spin density on the pendant side chain, and indicates charge transfer between the excited QD and the attached dopamine[9]. When βME was added to the solution, the intensity of the DA^+ signal decreased drastically, confirming that the presence of the antioxidant suppressed the oxidation of dopamine. There was no immediate qualitative difference between the green and yellow QDs, but in samples aged >1 h, more oxidized dopamine was generated from the green QDs (see Supplementary Information, Fig. S3).

Time-resolved emission spectroscopy using time-correlated single-photon counting (TCSPC) was then used to track electron and hole transfer between the QDs and the other components of the medium. The advantage of this technique is that it can indicate the transfer of either electrons or holes[10], enabling us to identify qualitative differences between freshly prepared conjugates of green and yellow QDs (corresponding to the steady-state spectra in Fig. 1a). In the absence of βME, both colours of QDs showed similar effects: faster initial decay and very little contribution from the long-time components, corresponding to steady-state quenching (Fig. 2b). In the presence of βME, green-emitting dopamine-conjugated QDs continued to show these features. This resulted in an overall reduction of area under the curve, or continued steady-state quenching. In contrast, yellow QD–dopamine showed an overall increase in area under the curve when βME was present, with restoration of long-time components to the values seen in unconjugated QDs (Fig. 2b and Supplementary Information, Table S1). This increase in the long-time tail results in the bright steady-state fluorescence observed in Fig. 1a for yellow QDs.

These differences in photophysics could be used to predict bioavailability and toxicity of the conjugates. The strong oxidized-dopamine peak on green QDs indicates electron transfer, but suggests that the conjugate will be cytotoxic, as the dopamine quinone is highly reactive and may even be formed during incubation in the dark (Fig. 3a). The limited amount of dopamine quinone generated with yellow QDs suggests little toxicity, but the rapid cap loss also suggests lowered bioavailability (Fig. 3b). The continued quenching of green QDs in the presence of βME suggests

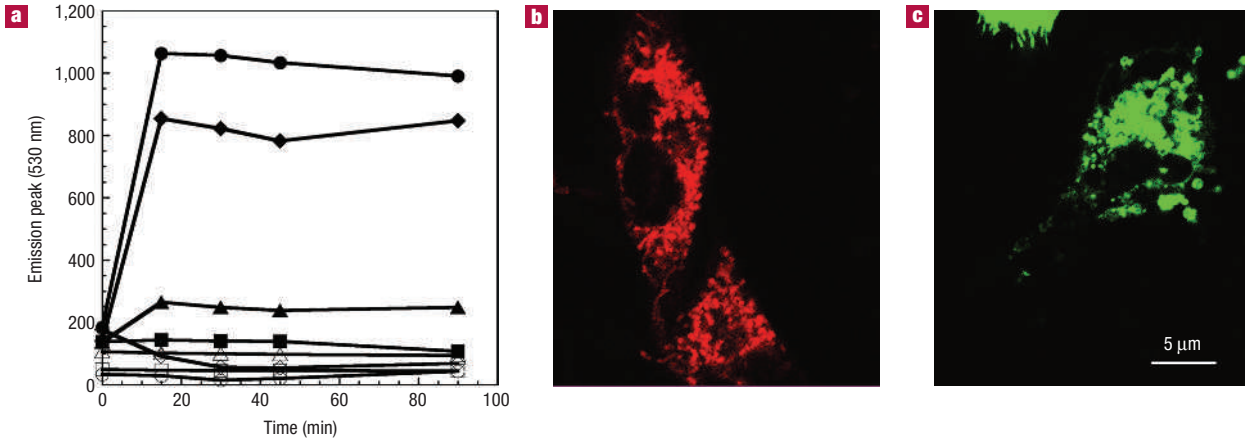

Figure 5 Singlet-oxygen generation and phototoxicity. a, The SOS fluorescence peak at 530 nm (excitation 504 nm) versus time, averaged over three experiments with error bars smaller than the symbols. A blank signal, consisting of SOS in water, was subtracted. The ultraviolet-irradiated samples are: QD–dopamine (QD–DA, filled circles); QD–dopamine with βME (QD−DA+βME, filled diamonds); MSA-solubilized QDs alone (QD, filled triangles); and QDs alone with βME (QD+βME, filled squares). Un irradiated samples do not differ substantially from each other, except for a slight reduction in levels in the presence of βME: MSA-solubilized QDs alone (open triangles); QD–dopamine (open circles); QD–dopamine with βME (open diamonds); and QDs alone with βME (open squares). **b**, Confocal micrograph of a healthy cell labelled with MitoTracker Red. The filamentous structure of the mitochondria is typical (scale as for **c**). **c**, The rounded mitochondria seen in this cell labelled with green QD–dopamine in the presence of βME are a classic sign of oxidative damage. This cell was found in a region illuminated with a Hg lamp through a DAPI filter set for 15 min.

that electron transfer continues between QDs and dopamine in this case, leading to particles capped with reduced, non-toxic dopamine (Fig. 3c). For yellow QDs, the TCSPC results suggest that βME probably reacts directly with the QD surface after loss of dopamine ligands, eliminating electron traps and increasing fluorescence quantum yield by lengthening lifetimes. This phenomenon has been observed and confirmed in time-resolved studies of QDs exposed to βME alone[10]. This leads to QDs that are fluorescent but poorly available for specific binding to dopamine receptors (Fig. 3d).

Bioavailability may be predicted to result from specific binding. In cells bearing dopamine receptors, the reduced form of dopamine will be recognized by dopamine receptors due to hydrogen bonding between the hydroxyls and specific serines of the receptor[11] (Fig. 3e). For the oxidized form, the quinone will bind any cysteine sulphhydryl (Fig. 3f); there is one cysteine within the dopamine-receptor-recognition site[12], as well as on many other proteins.

Uptake into cultured mammalian cell lines was studied to confirm these predictions. Recognition by dopamine receptors was expected to lead to receptor-mediated endocytosis in cell lines bearing these receptors. As expected, no uptake of these conjugates was seen in cells without dopamine receptors, which is consistent with studies showing that QDs conjugated to specific ligands do not bind cells non-specifically[13]. This should be distinguished from the often massive QD uptake that is seen with non-specific binding of surface caps to membrane structures, and which is particularly efficient when the QDs are positively charged at physiological pH, allowing them to bind to negatively charged cell-surface glycoproteins and glycolipids[14,15].

In cells stably expressing human D2 dopamine receptors, green QD–dopamine was assimilated readily, and toxic effects were severe. After 1 h of incubation in the dark, a significant thinning of the cell population was seen, indicating that cells had died and detached from the dish. Those that remained had blebbed, irregular membranes, typical of oxidative damage (Fig. 4a–d). Labelling with SYTOX Green revealed that >90% of the cells had compromised membranes, and labelling with dihydroethidium (DHE) showed red nuclei indicating the presence of reactive oxygen species in 100% of the cells (not shown; see Supplementary Information).

The addition of βME to the culture medium of labelled cells prevented dopamine quinone formation and enhanced labelling. A concentration of 5.7 mM reduced the number of SYTOX-Green-positive cells to <5% and the number of DHE-positive cells to <20% on initial examination. Cell survival and morphology remained normal throughout the incubation for imaging periods up to 20 min. Fluorescent labelling was intense and low-background, labelling primarily the perinuclear region, with the non-organelle cytoplasmic areas remaining free of QDs (Fig. 4e–h). However, phototoxicity could be induced by Hg lamp or laser illumination for 5–20 min. This was observable as 100% DHE-positive and >80% SYTOX-positive cells in the illuminated regions (data not shown; $n = 5$ dishes, see Supplementary Information).

Uptake could be prevented by a 10-fold excess of unlabelled dopamine; in this case, large clusters of unassimilated QDs were seen in the background after washing, with little association with cells (Fig. 4i,j). In contrast, in cells that lacked dopamine receptors (HEK293 and 3T3 cells), the QDs did not adhere to the cells and were completely washed away, leading to a black background (data not shown).

Greatly reduced toxicity was seen with yellow QD–dopamine, even in the absence of βME (<20% membrane-damaged cells after 1 h) and in the presence of light (no significant change in SYTOX staining in irradiated regions after 20 min, $n = 4$ dishes). Rates of assimilation were significantly reduced compared with the green QD conjugates, with most of the yellow QD–dopamine forming insoluble aggregates that adhered to cells and were not removed by washing, but which showed no signs of being taken up into endosomes (Fig. 4k–m).

Thus, there are two distinct mechanisms of cytotoxicity: dopamine quinone toxicity, which may occur in the dark and which is eliminated by βME, and phototoxicity, which occurs only with irradiation of the QDs and is not entirely prevented by βME. The mechanism of phototoxicity was investigated several ways. First, we tested QD conjugates for generation of singlet oxygen ($^1O_2$).

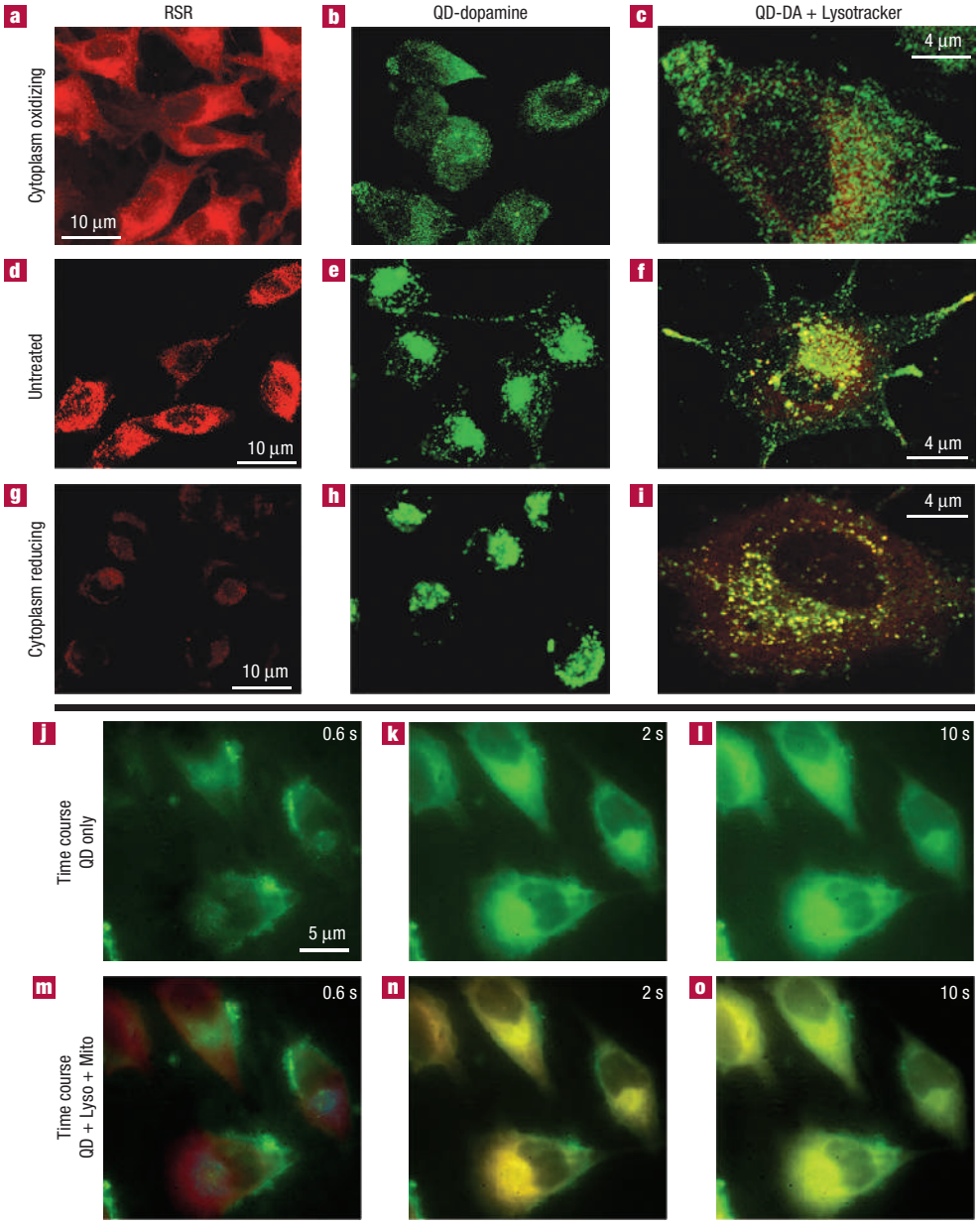

Figure 6 Redox-sensitive labelling with QD–dopamine and comparison with commercial redox sensor dye RSR. All experiments were carried out with green QDs in the presence of βME. **a**, Cells under the most oxidizing conditions (10 mM BSO) labelled with RSR alone. **b**, Cells under the most oxidizing conditions labelled with QD–dopamine alone. Note that both RSR and QDs are fluorescent throughout the cell, excluding the nucleus. Scale bar as for **a**. **c**, High-power image of cells under the most oxidizing conditions labelled with QD–dopamine and LysoTracker Red. Note the weak red staining and very few punctae, suggesting lysosomal rupture. **d**, Untreated, actively proliferating cells labelled with RSR, showing distribution to mitochondria and lysosomes. **e**, With QD–dopamine, a large perinuclear 'cap' is observed in untreated cells, with some staining throughout the rest of the cell; the filamentous structures suggest mitochondria. Scale bar as for **d**. **f**, Co-labelling with QDs and LysoTracker shows that the bright cap corresponds to lysosomes, and that QDs do not enter the nucleus; note the large amount of perinuclear staining that is only green (not lysosomal) and which corresponds mostly to mitochondria (see Supplementary Information, Fig. S4). **g**, Cells made more reducing (1 mM GSH-MEE) and labelled with RSR, which is weak and is restricted to lysosomes. **h**, Reducing cells with QD–dopamine have a similar appearance to **g**. Scale bar as for **g**. **i**, High-resolution inspection of LysoTracker–QD-co-labelled reducing cells shows very little fluorescence from QDs alone (green) and many bright co-labelled punctae (yellow): thus, essentially all of the QD fluorescence is lysosomal. **j**, Epifluorescence, non-confocal image of a QD–dopamine labelled cell after the minimal amount of ultraviolet exposure required to obtain a full spectrum (600 ms). Note the round regions similar to the pattern in **g**,**h**. **k**, After 2 s of total exposure, overall labelling has brightened and areas of the cell previously dark have become apparent. **l**, Few quantitative changes occur in the cell labelling pattern after 2 s of exposure. **m**, Cells in **j** co-labelled with LysoTracker Blue and MitoTracker Red. Note the QD overlap with lysosomal staining but not mitochondrial staining. **n**, After 2 s, LysoTracker staining has faded and QD and MitoTracker labelling overlap almost completely. **o**, After 10 s of exposure, MitoTracker has faded, whereas the QDs have continued to brighten.

Although neither the electron nor the hole of unconjugated CdSe/ZnS is expected to be energetic enough to generate free radicals[16], a QD may transfer energy to another molecule capable of generating $^1O_2$ (a 'photosensitizer'). This mechanism has been proposed as a method for the creation of phototoxic drugs for the destruction of cancer cells[17,18]. Oxidation of dopamine has been confirmed to generate $^1O_2$ (ref. 19), and thus dopamine is a probable photosensitizer given the electron-transfer processes confirmed here. We quantified singlet oxygen in solution using Singlet Oxygen Sensor Green (SOS) reagent, which is unresponsive to other oxidants (unlike DHE, which labels all reactive oxygen species). QD–dopamine was compared with mercaptosuccinic acid (MSA)-solubilized QDs alone. $^1O_2$ formation was dependent on ultraviolet irradiation, and occurred rapidly with QD–dopamine in both the presence and absence of βME, reaching >90% of the final levels within 10 min. QDs alone did not generate significant levels of $^1O_2$, even after >1 h of ultraviolet exposure (Fig. 5a). Correspondingly, prolonged imaging of QD–dopamine cells led to alterations in mitochondrial morphology consistent with oxidative damage (Fig. 5b,c).

Because reactive oxygen species are capable of nicking DNA *in vitro*, we then tested for oxidative damage to DNA in genomic material extracted from these cells. A quantitative assay for OH-hydroxyguanine revealed no significant differences between the number of abasic sites in QD–dopamine-exposed cells versus controls, even after 20 min of irradiation (<1 site found in all samples; $n = 3$ for each of the controls, QD–dopamine irradiated and unirradiated, QD–dopamine with βME irradiated and unirradiated).

Cd^{2+} release is another possible source of cytotoxicity. Using ion chromatography–mass spectrometry, our detection limits were in the p.p.t. range, making Cd concentrations in our samples easily quantifiable. In QD-560–dopamine conjugates, we found Cd concentrations of 114 p.p.b. for non-irradiated samples and 222 p.p.b. after 2 h of ultraviolet irradiation in the presence of air and water ($n = 5$). In the presence of βME, levels of free Cd fell nearly to detection limits, probably because of Cd-thiol complex formation. Levels were 14 p.p.b. in non-irradiated samples and 15 p.p.b. in irradiated samples ($n = 5$). The toxic threshold for cells is consistently reported to be in the tens of p.p.m. range[20]. Our results are consistent with previous studies[21], where significant cytotoxicity and high levels of free Cd were only reported with bare-core CdSe particles. With CdSe/ZnS QDs, 8 h of ultraviolet exposure were required to produce significant effects on cells. Another study confirmed the protective effect of the ZnS shell[22], and both studies suggested additional protective effects of ligands added to the conjugation shell. Thus, it is not surprising that our QD–dopamine conjugates did not show significant Cd release within the timescales of our labelling experiments.

The 'unquenching' observed in Fig. 1c suggested that the redox environment surrounding the QD–dopamine conjugates could influence their fluorescence, thus making them a potentially useful redox probe. Cellular redox sensors, such as the commercial dye RedoxSensor Red (RSR), give information about a cell's redox state by their pattern of distribution within the cell. RSR is non-fluorescent until oxidized; thus, in a cell with a highly reducing cytoplasm, only the lysosomes will provide a sufficiently oxidizing environment to render the dye visible. Under normal conditions of cell proliferation, RSR is visible in lysosomes and mitochondria[23]. Co-labelling with QD–dopamine and RSR is not effective, as RSR quenches QD fluorescence (tested both in solution and in cells; see Supplementary Information, Fig. S4). However, the two dyes could be used in parallel to compare labelling patterns.

Cell cultures with different intracellular redox potentials were generated by enhancing or suppressing glutathione: glutathione monoethyl ester (GSH-MEE) makes the cellular environment more reducing, and L-buthionine-sulphoximine (BSO) makes it more oxidizing by suppressing glutathione synthesis[24]. Alteration of the cellular redox potential greatly changed QD-labelling patterns in a fashion similar to that seen with RSR. Under the most oxidizing conditions tested—in the presence of 10 mM BSO—RSR was oxidized directly in the cytoplasm, leading to staining of the entire cell (Fig. 6a). QD–dopamine fluorescence was also found throughout all regions of the cell except the nucleus (Fig. 6b,c). In untreated cells, RSR was seen surrounding cell nuclei, corresponding to lysosomes and mitochondria (Fig. 6d). The QD–dopamine pattern was similar to that with RSR (Fig. 6e), and escape from lysosomes was confirmed by co-labelling with LysoTracker Red (Fig. 6f). When the cellular environment was made more reducing, which could be accomplished with as little as 0.1 mM GSH-MEE, RSR fluorescence was very weak and restricted to lysosomes (Fig. 6g). QD–dopamine fluorescence, although brighter, was also restricted to a lysosomal 'cap' that showed almost complete overlap with LysoTracker staining (Fig. 6h,i).

If the cells were carefully protected from ultraviolet exposure before initial imaging (by focusing under brightfield), it could be seen that high-intensity ultraviolet was equivalent to suppression of glutathione in its effects on QD–dopamine fluorescence, appearing as a 'migration' of labelled areas of the cells. On initial imaging, the areas near the lysosomes were fluorescent immediately (~100 ms exposure), and the perinuclear region was dark. Labelling of the perinuclear region appeared rapidly, after 0.5–2 s of exposure, showing a time course similar to that in Fig. 1d. As irradiation continued, the lysosomal region dimmed first, with the perinuclear region remaining bright and some fluorescence appearing in the cytoplasm (Fig. 6j–o) (see Supplementary Information, Video S1). Once stabilized, fluorescence remained stable under normal illumination conditions for at least 10 min (not shown; $n > 50$). In fixed cells, enhancement was slow and limited, showing brightening predominantly in lysosomes (see Supplementary Information, Video S2).

This work provides a general framework for the creation of probes that label different areas of living cells according to their redox state. Quenching of reduced QDs, followed by unquenching under continued light exposure or in oxidizing environments, provides a visible signal with a slow enough time course to be readily quantified. QD–dopamine with βME is a viable alternative or complement to the redox-sensitive dye RSR, showing much greater photostability, and can be used to monitor glutathione function and photooxidation. The use of other QD–electron-donor conjugates for this purpose remains to be established. This opens a new avenue of research that may lead to the development of redox-sensitive probes that can be targeted to specific cell populations bearing the appropriate receptors.

These results also suggest that catechols may serve as useful sensitizers for QD photodynamic therapy. As a more general rule, any electron donor that efficiently quenches QD emission should act as a photosensitizer in cells bearing receptors to that donor. We have previously reported quenching-dependent uptake of QD–adenine in bacteria through oxidation-generated membrane defects[25], suggesting that this principle can be generalized to many different biological systems and applications.

METHODS

CdSe/ZnS QDs were synthesized, characterized, and conjugated to dopamine using the activator *N*-(3-dimethylaminopropyl)-*N'*-ethylcarbodiimide (EDC) as described[6,26]. Solubilization was carried out with MSA as published[27]; briefly, 20 mg of MSA was added to 5 mg of trioctylphosphine oxide (TOPO) capped QDs suspended in 25 ml methanol. The pH was adjusted to 10.6 using

tetramethylammonium hydroxide pentahydrate and the mixture was heated at 65 °C under Ar for 6 h.

Conjugates to dopamine were prepared in a glove bag under Ar gas to prevent oxidation of dopamine by the atmosphere; conjugates were kept under Ar until immediately before use. Two colours of QDs were used in all experiments: green-emitting (peak 560 nm) and yellow-emitting (peak 590 nm). For ultraviolet–visible stability experiments, two additional colours were used, with peaks at 570 and 600 nm. Preparation and characterization of conjugates is described in the Supplementary Information.

Emission spectra were taken on a Gemini EM fluorescence plate reader (SpectraMax); excitation was at 400 nm unless stated otherwise. Absorbance spectra were taken on a SpectraMax Plus (Molecular Devices). The generation of singlet oxygen was assayed in the plate reader using 1 μM SOS (Molecular Probes) with excitation at 504 nm and emission at 514–600 nm. QD concentrations ranged from 6–150 nM in 20–50 nM increments. Duplicate samples were prepared for each condition, one to be ultraviolet-exposed and the other aged under room oxygen but not ultraviolet-exposed. The unexposed side of the plate was screened with aluminium foil.

QD–dopamine uptake was studied in mammalian cell lines. Details of the procedures for culture and labelling are given in the Supplementary Information. Epifluorescence images and steady-state emission spectra from cultured cells and cell-free controls were taken on an Olympus IX-71 microscope equipped with a Nuance multispectral imaging system (including a visible liquid-crystal filter tunable between 420 and 750 nm in 10 nm increments) (Cambridge Research Instruments). Epifluorescence illumination was through a 'quantum dot' filter cube set (excitation = 380–460 nm, dichroic 475 nm, emission = 500 longpass (LP); Chroma filter 32013). To visualize oxidized dopamine, a 4,6-diamidino-2-phenylindole (DAPI) filter set was used (excitation = 350/50 nm, dichroic 400 nm, emission = 440 LP).

Images were taken of cells incubated with QDs alone, as well as of cells co-incubated with selected dyes. All dyes were purchased from Molecular Probes, and were added 30 min after the beginning of incubation with the QDs, and were allowed to remain on the cells for 30 min before washing. The dyes and concentrations used were: the nuclear stain SYTO Red (5 μM), the nuclear stain for membrane-compromised cells SYTOX Green (1 μM), the oxidative sensor dihydroethidium (DHE; 5 μM), the lysosomal indicator LysoTracker Red or LysoTracker Blue (1 μM), the mitochondrial indicator MitoTracker Red (1 μM), and the redox sensitive dye RSR (1 μM). In some cells, LysoTracker Blue and RSR or MitoTracker Red were used together. Quantification of quenching of QD fluorescence by RSR, and the use of DHE and SYTOX for toxicity testing are described in the Supplementary Information.

To alter intracellular redox potentials, cells were treated with 0.1, 1 or 10 mM GSH-MEE and BSO in Dulbecco's modified Eagle medium for 4 h. Following this treatment, the cells were washed, and QDs and dyes were added as above.

Confocal imaging of redox-labelled cells was carried out on a Zeiss 510 LSM with a PlanApo ×100 oil objective. QDs were excited with an Ar ion laser (458 nm line); LysoTracker Red and RSR were excited with a HeNe laser (543 nm line). Cells labelled with >1 probe were examined for channel bleed-through before imaging. When RedoxSensor was used, it was located under brightfield and imaged first to avoid photooxidation and migration of the dye[23]. LysoTracker Blue and DHE were visualized under a DAPI filter.

TCSPC was used for transient emission measurements. We previously published the full procedure[6]. Samples were transferred to a cuvette under nitrogen in the dark. TCSPC measurements were taken with emission detected at 560 nm at the magic angle with respect to the 400 nm excitation laser polarization. Data were analysed using AxoGraph (Axon Instruments) and a custom Levenberg–Marquardt multi-exponential fitting routine[28].

The methods for quantification of DNA damage, ion chromatography–mass spectrometry, and EPR spectroscopy are given in the Supplementary Information.

Received 20 October 2005; accepted 8 March 2006; published 16 April 2006.

References

1. Anderson, N. A. & Lian, T. Ultrafast electron transfer at the molecule-semiconductor nanoparticle interface. *Annu. Rev. Phys. Chem.* **56,** 491–519 (2005).
2. Dimitrijevic, N. M., Saponjic, Z. V., Rabatic, B. M. & Rajh, T. Assembly and charge transfer in hybrid TiO(2) architectures using biotin-avidin as a connector. *J. Am. Chem. Soc.* **127,** 1344–1345 (2005).
3. Ginger, D. S. & Greenham, N. C. Photoinduced electron transfer from conjugated polymers to CdSe nanocrystals. *Phys. Rev. B* **59,** 10622–10629 (1999).
4. Nozik, A. J. Quantum dot solar cells. *Physica E* **14,** 115–120 (2002).
5. Landes, C., Burda, C., Braun, M. & El-Sayed, M. A. Photoluminescence of CdSe nanoparticles in the presence of a hole acceptor: n-butylamine. *J. Phys. Chem. B* **105,** 2981–2986 (2001).
6. Kloepfer, J. A., Bradforth, S. & Nadeau, J. L. Photo-physical properties of biologically compatible CdSe quantum dot structures. *J. Phys. Chem. B* **109,** 9996–10003 (2005).
7. Lakowicz, J. R. *Principles of Fluorescence Spectroscopy* (Plenum, New York, 1999).
8. Aldana, J., Lavelle, N., Wang, Y. J. & Peng, X. G. Size-dependent dissociation pH of thiolate ligands from cadmium chalcogenide nanocrystals. *J. Am. Chem. Soc.* **127,** 2496–2504 (2005).
9. Rajh, T. *et al.* Surface restructuring of nanoparticles: An efficient route for ligand-metal oxide crosstalk. *J. Phys. Chem. B* **106,** 10543–10552 (2002).
10. Jeong, S. *et al.* Effect of the thiol-thiolate equilibrium on the photophysical properties of aqueous CdSe/ZnS nanocrystal quantum dots. *J. Am. Chem. Soc.* **127,** 10126–10127 (2005).
11. Floresca, C. Z. & Schetz, J. A. Dopamine receptor microdomains involved in molecular recognition and the regulation of drug affinity and function. *J. Recept. Signal. Transduct. Res.* **24,** 207–239 (2004).
12. Javitch, J. A., Li, X., Kaback, J. & Karlin, A. A cysteine residue in the third membrane-spanning segment of the human D2 dopamine receptor is exposed in the binding-site crevice. *Proc. Natl Acad. Sci. USA* **91,** 10355–10359 (1994).
13. Pinaud, F., King, D., Moore, H. P. & Weiss, S. Bioactivation and cell targeting of semiconductor CdSe/ZnS nanocrystals with phytochelatin-related peptides. *J. Am. Chem. Soc.* **126,** 6115–6123 (2004).
14. Lovric, J. *et al.* Differences in subcellular distribution and toxicity of green and red emitting CdTe quantum dots. *J. Mol. Med.* **83,** 377–385 (2005).
15. Parak, W. J., Pellegrino, T. & Plank, C. Labelling of cells with quantum dots. *Nanotechnology* **16,** R9–R25 (2005).
16. Ipe, B. I., Lehnig, M. & Niemeyer, C. M. On the generation of free radical species from quantum dots. *Small* **1,** 706–709 (2005).
17. Samia, A. C. S., Chen, X. B. & Burda, C. Semiconductor quantum dots for photodynamic therapy. *J. Am. Chem. Soc.* **125,** 15736–15737 (2003).
18. Bakalova, R. *et al.* Quantum dot anti-CD conjugates: Are they potential photosensitizers or potentiators of classical photosensitizing agents in photodynamic therapy of cancer?. *Nano Lett.* **4,** 1567–1573 (2004).
19. Lichszteld, K., Michalska, T. & Kruk, I. Identification by Esr spectroscopy and spectrophotometry of singlet oxygen, formed during autoxidation of catecholamines. *Z. Phys. Chem.* **175,** 117–122 (1992).
20. Limaye, D. A. & Shaikh, Z. A. Cytotoxicity of cadmium and characteristics of its transport in cardiomyocytes. *Toxicol. Appl. Pharmacol.* **154,** 59–66 (1999).
21. Derfus, A. M., Chan, W. C. W. & Bhatia, S. N. Probing the cytotoxicity of semiconductor quantum dots. *Nano Lett.* **4,** 11–18 (2004).
22. Kirchner, C. *et al.* Cytotoxicity of colloidal CdSe and CdSe/ZnS nanoparticles. *Nano Lett.* **5,** 331–338 (2005).
23. Chen, C. S. & Gee, K. R. Redox-dependent trafficking of 2,3,4,5,6-pentafluorodihydrotetramethylrosamine, a novel fluorogenic indicator of cellular oxidative activity. *Free Radic. Biol. Med.* **28,** 1266–1278 (2000).
24. Anderson, M. E. Glutathione: an overview of biosynthesis and modulation. *Chem. Biol. Interact.* **111–112,** 1–14 (1998).
25. Kloepfer, J. A., Mielke, R. E. & Nadeau, J. L. Uptake of CdSe and CdSe/ZnS quantum dots into bacteria via purine-dependent mechanisms. *Appl. Environ. Microbiol.* **71,** 2548–2557 (2005).
26. Kloepfer, J. A. *et al.* Quantum dots as strain- and metabolism-specific microbiological labels. *Appl. Environ. Microbiol.* **69,** 4205–4213 (2003).
27. Chen, Y. F., Ji, T. H. & Rosenzweig, Z. Synthesis of glyconanospheres containing luminescent CdSe-ZnS quantum dots. *Nano Lett.* **3,** 581–584 (2003).
28. Press, W. H., Flannery, B. P., Teukolsky, S. A. & Vetterling, W. T. *Numerical Recipes in Fortran* (Cambridge Univ. Press, New York, 1992).
29. Aldana, J., Wang, Y. A. & Peng, X. G. Photochemical instability of CdSe nanocrystals coated by hydrophilic thiols. *J. Am. Chem. Soc.* **123,** 8844–8850 (2001).

Acknowledgements

This research is supported by the United States EPA—Science to Achieve Results (STAR) program Grant No. R831712, and by the Canadian Institutes of Health Research (CIHR) Grant No. PPP-71486. S.J.C. acknowledges support from The Banting Research Foundation. N.M.D. is supported by the Office of Basic Energy Sciences, Division of Chemical Sciences, US-DOE under contract number W-31-109-Eng-38. The TCSPC work carried out at USC is supported by the David and Lucile Packard Foundation and NASA-JPL instrument contract 1 250 277.
Correspondence and requests for materials should be addressed to J.L.N.
Supplementary Information accompanies this paper on www.nature.com/naturematerials.

Competing financial interests

The authors declare that they have no competing financial interests.